



5-Aryl-1*H*-pyrazole-3-carboxylic acids as selective inhibitors of human carbonic anhydrases IX and XII



Ilija N. Cvijetić^a, Muhammet Tanç^b, Ivan O. Juranić^c, Tatjana Ž. Verbić^d, Claudiu T. Supuran^{b,*}, Branko J. Drakulić^{c,*}

^a Innovation Center of the Faculty of Chemistry, University of Belgrade, Studentski Trg 12-16, 11000 Belgrade, Serbia

^b NEUROFARBA Department, Sezione di Scienze Farmaceutiche e Nutraceutiche, Università degli Studi di Firenze, Via Ugo Schiff 6, 50019 Sesto Fiorentino, Florence, Italy

^c Department of Chemistry, Institute of Chemistry, Technology and Metallurgy, University of Belgrade, Njegoševa 12, 11000 Belgrade, Serbia

^d Faculty of Chemistry, University of Belgrade, Studentski Trg 12-16, 11000 Belgrade, Serbia

ARTICLE INFO

Article history:

Received 15 April 2015

Revised 26 May 2015

Accepted 29 May 2015

Available online 4 June 2015

Keywords:

Carbonic anhydrase

Phenyl-pyrazole-carboxylic acids

Docking

Molecular interaction fields

Active sites comparison

ABSTRACT

Inhibitory activity of a congeneric set of 23 phenyl-substituted 5-phenyl-pyrazole-3-carboxylic acids toward human carbonic anhydrase (hCA, EC 4.2.1.1) isoforms I, II, IX and XII was evaluated by a stopped-flow CO₂ hydrase assay. These compounds exerted a clear, selective inhibition of hCA IX and XII over hCA I and II, with K_i in two to one digit micromolar concentrations (4–50 μM). Derivatives bearing bulkier substituents in *para*-position of the phenyl ring inhibited hCA XII at one-digit micromolar concentrations, while derivatives having alkyl substituents in both *ortho*- and *meta*-positions inhibited hCA IX with K_i s ranging between 5 and 25 μM. Results of docking experiments offered a rational explanation on the selectivity of these compounds toward CA IX and XII, as well as on the substitution patterns leading to best CA IX or CA XII inhibitors. By examining the active sites of these four isoforms with GRID generated molecular-interaction fields, striking differences between hCA XII and the other three isoforms were observed. The field of hydrophobic probe (DRY) appeared significantly different in CA XII active site, comparing to other three isoforms studied. To the best of our knowledge such an observation was not reported in literature so far. Considering the selectivity of these carboxylates towards membrane-associated over cytosolic CA isoforms, the title compounds could be useful for the development of isoform-specific non-sulfonamide CA inhibitors.

© 2015 Elsevier Ltd. All rights reserved.

1. Introduction

There are a few reports on biological activity of 5-aryl-pyrazole-3-carboxylic acid in the literature. Compounds were described as partial agonists of the nicotinic acid receptors,¹ as inhibitors of replication protein A protein–protein interactions,² as scaffolds that lead to inhibitors of protein tyrosine phosphatase 1B,³ and as an inhibitors of a tissue-nonspecific alkaline phosphatase.⁴ Along with this, 5-heteroaryl-pyrazole-3-carboxylic acids, among other compounds, were recently described as inhibitors of human carbonic anhydrases (CAs, EC 4.2.1.1) I, II, IX and XII.⁵

Abbreviations: CA, carbonic anhydrase; ZBG, zinc binding group; CAIs, carbonic anhydrase inhibitors; pK_a , acid dissociation constant; K_i , inhibition constant; PDB, Protein Data Bank; MIFs, molecular interaction fields; HBD, hydrogen bond donor; HBA, hydrogen bond acceptor.

* Corresponding authors. Tel.: +39 055 4573005 (C.T.S.); tel.: +381 11 3336741 (B.J.D.).

E-mail addresses: claudiu.supuran@unifi.it (C.T. Supuran), bdrakuli@chem.bg.ac.rs (B.J. Drakulić).

The majority of reported small molecule CA inhibitors (CAIs) comprises a primary sulfonamide moiety as a zinc binding group (ZBG). The sulfonamide anion ($-\text{SO}_2\text{NH}^-$) coordinates the active site Zn²⁺ ion and blocks catalysis. In Protein Data Bank more than 300 unique sulfonamide-bearing small molecules co-crystallized with carbonic anhydrases (mainly human isoform II) can be found. On the other hand, significantly less non-sulfonamide CAIs, belonging to other classes of small organic molecules, such as for example carboxylic acids, were investigated so far. It was shown that some molecules comprising $-\text{COOH}$ moiety co-crystallized with different CA isoforms, are bound within the CA active site, interacting with the active site Zn²⁺ by water-mediated H-bonding, while other were found bound to the enzyme but did not interact with the active site Zn²⁺ ion, or they were bound out of the active site. Best examples of the latter are, probably, *ortho*-hydroxy cinnamic acids—mechanism-based inhibitors originated in situ by hydrolysis of coumarins by Zn²⁺—hydroxyl ion couple in the CA active site.^{6–9} Isoform selectivity of this class of compounds depends on substitution pattern on coumarin phenyl ring. Recently reported

2-benzylsulfinylbenzoic acid¹⁰ was found bound to hCA II out of the active site. This compound constrained the proton-shuttle residue His64 in its 'out' conformation by a network of water molecule-mediated H-bonds. Inhibition study of hCA I and II, as well as mycobacterial and fungal CA with a library of natural products, found adduct of cinnamic and maleic acid amide, 3-(3-chloro-4-hydroxyphenyl)-2-[(4-methoxy-4-oxobut-2-enoyl)amino]propanoic acid (CID 72785959, CAS 852690-88-1), as a low micromolar CA inhibitor.¹¹ Structure of compound co-crystallized with hCA II revealed that carboxyl group of cinnamic acid moiety is not involved in interaction with catalytic Zn²⁺ ion. Inhibition of mycobacterial CA Rv3588c by (+)-mispyric acid, natural product bearing two carboxyl groups, was also described,¹² without additional structural data. Smaller carboxylate-bearing molecules, such as hydroxy and thio-substituted benzoic acids, were found bound to the CA active site, forming hydrogen bond to the Zn-bound water molecule/hydroxide ion.¹³ In the same crystal structures two more molecules of substituted benzoic acids were found, occupying protein cavities out of the binding site. Inhibition of CAs with biologically-relevant aliphatic carboxylates, along with benzoic and 1,2,5,6-tetrafluoro-benzoic acids were also described, without additional structural data.¹⁴ A congeneric set of di-methoxy-bromophenyl-substituted 2-benzyl-cyclopropyl carboxylic acids and derivatives, having the same topological distance between aryl and carboxyl moieties as in a title compounds, were recently reported as inhibitors of human CA isoforms I, II, IX and XII.¹⁵ Those compounds exerted strong preferences toward hCA I and II inhibition. Carboxylic acid derivatives briefly described in the previous lines inhibited CAs with K_s spanning range between the millimolar to micromolar concentrations, with the exception of 2-benzyl-cyclopropyl carboxylic acids, found as nanomolar inhibitors.

In this article we report the synthesis and inhibitory activity of a congeneric set of 23 phenyl-substituted 5-phenyl-pyrazole-3-carboxylic acids (**1–23**) toward human CA isoforms I, II, IX and XII.

2. Results and discussion

2.1. Chemistry

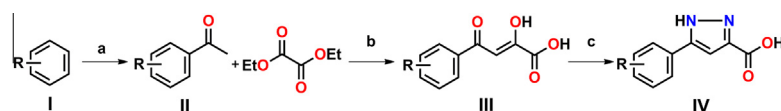
The rationale of this work was to investigate different chemotypes incorporating the COOH moiety as a ZBG for obtaining CAIs. As heterocyclic carboxylic acids were rarely investigated as CAIs, we decided to synthesize a congeneric series of such derivatives incorporating the synthetically easily available pyrazole-3-carboxylic acid moiety.

Acetophenones **II** were prepared by Friedel–Crafts acylation of the corresponding aromatic substrates (**I**), or commercially available substances were used. The aryl-diketo acids **III** were prepared following previously reported procedures,¹⁶ by base-promoted condensations of substituted acetophenones (**II**) and diethyl-oxalate. Compounds **1–23** (**IV**) were synthesized from aryl-diketo acids (**III**) and hydrazine-hydrate in glacial acetic acid (Scheme 1).

Identity and purity of compounds was confirmed by ¹H and ¹³C NMR spectroscopy and LC-HR/ESI-MS.

2.2. Tautomeric preferences and protonation states

Aryl-pyrazole-carboxylic acid could appear in three tautomeric forms (Scheme 2).



Scheme 1. Synthesis of 5-aryl-1H-pyrazole-3-carboxylic acids. (a) CH₃COCl, AlCl₃/CH₂Cl₂, 6 h, 0 °C to rt; (b) 2 equiv Na/CH₃OH, 15^h, rt, then conc. HCl, (c) N₂H₄·H₂O/CH₃COOH, 8^h, rt.

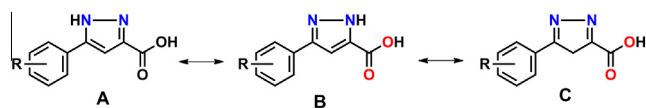
Tautomers A and B, with protonated pyrazole nitrogens, are more probable than the tautomer C. In solid state, tautomeric form A was observed.¹⁷ To gather more data on tautomeric preferences of examined compounds in solution, we recorded NOESY spectra of 4-Me-derivative (**1**), in DMSO-*d*₆. 4-Me-derivative (**1**) was chosen because of simple ¹H NMR pattern of protons on phenyl ring. Spectra were recorded in DMSO due to good solubility of examined compounds and its polarity, which preclude possible aggregation of solute by intramolecular H-bonding, observed in solid state (see below). Clear NOESY signal between broad ¹H peak at 13.38 ppm and doublet at 7.71 ppm (Fig. 1) was observed.

Doublet at 7.71 ppm belongs to hydrogens in *ortho*-position of the phenyl ring, while broad signal at 13.38 ppm belongs to pyrazole NH. Those data suggested that tautomer A is principal one in DMSO solution. Upon addition of one molar equivalent of piperidine, to deprotonate carboxyl group, broad signal at 13.38 ppm was shifted to 9.75 ppm and NOESY signal disappeared (Fig. S1 in Supplementary Material). Our preliminary results suggested that tautomeric form A should not be predominant one when carboxyl group of title compounds is in its anionic form, although it is well known that tautomeric preferences are different in different solvents. Tautomeric preferences of title compounds will be a subject of separate studies. IR spectra of compounds were obtained by ATR (attenuated total reflectance) from solid samples. In spectra of some compounds we clearly observed broad IR bands in the region 3100–3250 cm⁻¹, where NH stretching bands were overlapped with aromatic C–H bands. Such pattern in IR spectra suggested aggregation via hydrogen bonding of some derivatives. Examples are given in Supplementary Material, Figure S2. This is in accordance with crystal structure of unsubstituted derivative,¹⁷ where in crystal packing intermolecular H-bonds between carboxyl group and pyrazole –NH–N= part is observed. We also estimated protonation states¹⁸ of compound **1** (Fig. S3 in Supplementary Material). pK_a Value of carboxyl group is predicted to be within the range 3.6–4.0; while pK_a value of pyrazole nitrogen is predicted to be within the range 10.2–10.7, depending on tautomeric state (Fig. S4 in Supplementary Material). pK_{a1} Value (carboxyl group) of derivative **22** was experimentally determined using spectrophotometric titration. Three wavelengths used for spectrophotometric pK_{a1} determination (270, 280, 290 nm) were selected as wavelengths where the difference in absorptivity of species existing in the solution is maximal. The UV/Vis spectra and the graph used for the pK_{a1} value determination are shown in Figure 2. For details see Section 4. The determined pK_{a1} of derivative **22** is 3.31 ± 0.07.

2.3. CA inhibition

Inhibitory activity of compounds toward hCA I, II, IX and XII was evaluated by a stopped-flow CO₂ hydrase assay. Results are reported as K_i values (Table 1).

All compounds tested were proved to be inactive towards CA I and II, which were not inhibited up to concentrations of 50 μM inhibitor in the assay system. Depending on the substitution pattern on the phenyl ring, different subsets of compounds were active towards CA IX or towards CA XII. Along with K_i data reported in Table 1, strong selective inhibition of **1–23** toward CA IX and CA XII over CA I and II can be noted (see also Supplementary Table 1). Dose-response curves for inhibitory activity of these compounds



Scheme 2. Tautomers of aryl-pyrazole-carboxylic acids.

toward all CA isoforms appeared rather flat, still percentage of enzyme activity of CA I and II were between 60% and 70% even at 1×10^{-4} M concentrations of inhibitors. Providing selectivity toward membrane-associated CA isoforms, considered as a good anti-tumor targets,¹⁹ over cytosolic isoforms, the title compounds might be used as a good starting point for the design of isoform-selective inhibitors incorporating –COOH ZBGs. Compounds active toward CA IX and CA XII inhibited those two isoforms in one- to two-digit micromolar concentrations, comparable with the potency of the majority of so-far reported CA inhibitors bearing this ZBG.

2.4. Structure-activity study

In an attempt to explain selectivity of some of these compounds toward CA IX and CA XII and to explain preferences of different subsets of compounds toward CA IX or CA XII, we performed docking studies. For this purpose we chose Protein Data Bank (PDB) crystal structures derived from the wild-type CA isoforms and having a high resolution. CA I was modeled from PDB entry 1HCB, at 1.60 Å resolution²⁰; CA II from 3B4F, at 1.89 Å resolution²¹; CA IX from 3IAI, at 2.20 Å resolution²² and CA XII from 1JD0, at 1.50 Å resolution.²³ Some of those enzymes were co-crystallized with small molecule inhibitors. For the docking experiments we

removed all small molecules and waters, neutralized proteins with counter-ions, than embedded them in water clusters and relaxed all structures by molecular dynamics minimization (see Section 4 for details). In this point reasonable question arise: are minimization of the protein structure upon bound ligand removal can cause collapse of the active site? We believe that regarding CAs this possibility is not an issue. CAs poses a wide and conical active site in significant extent exposed to solvent. During catalytic cycle, that is, CO₂ hydration, small changes of protein conformation is observed, and such changes mainly can be attributed to the His64 (proton shuttle) conformation change. Consequently, different from some other enzyme classes, CAs in their crystal structures are not 'trapped' in some local free-energy minimum for which another, close, local minimum can exist. Additionally, majority of CA inhibitors are medium-sized molecules, which typically did not significantly change conformation of active site, comparing to uninhibited protein. By visual inspection of the 3D structures of very efficient inhibitors (typically nanomolar, from the sulfonamide class) cocrystallized with the CAs it can be observed that such molecules typically did not interact with its whole molecular surface with the active site residues. Most probably this can be attributed to the wide CAs active site, as well as to very high affinity of ZBG to catalytic Zn²⁺ ion. On the other hand, from the modelling set-up view, it should be noted that MD minimization (as far as recent CHARMM force field variants and recent NAMD releases are used) commonly very limited mobility of backbone appears, while position of side-chains are usually efficiently relaxed. In all so far reported crystal structures of CA co-crystallized with small molecules having a –COOH group within enzyme active site, the water molecule bound to catalytic Zn²⁺ ion was present. Thus, for the docking study we added this water molecule. Initial position

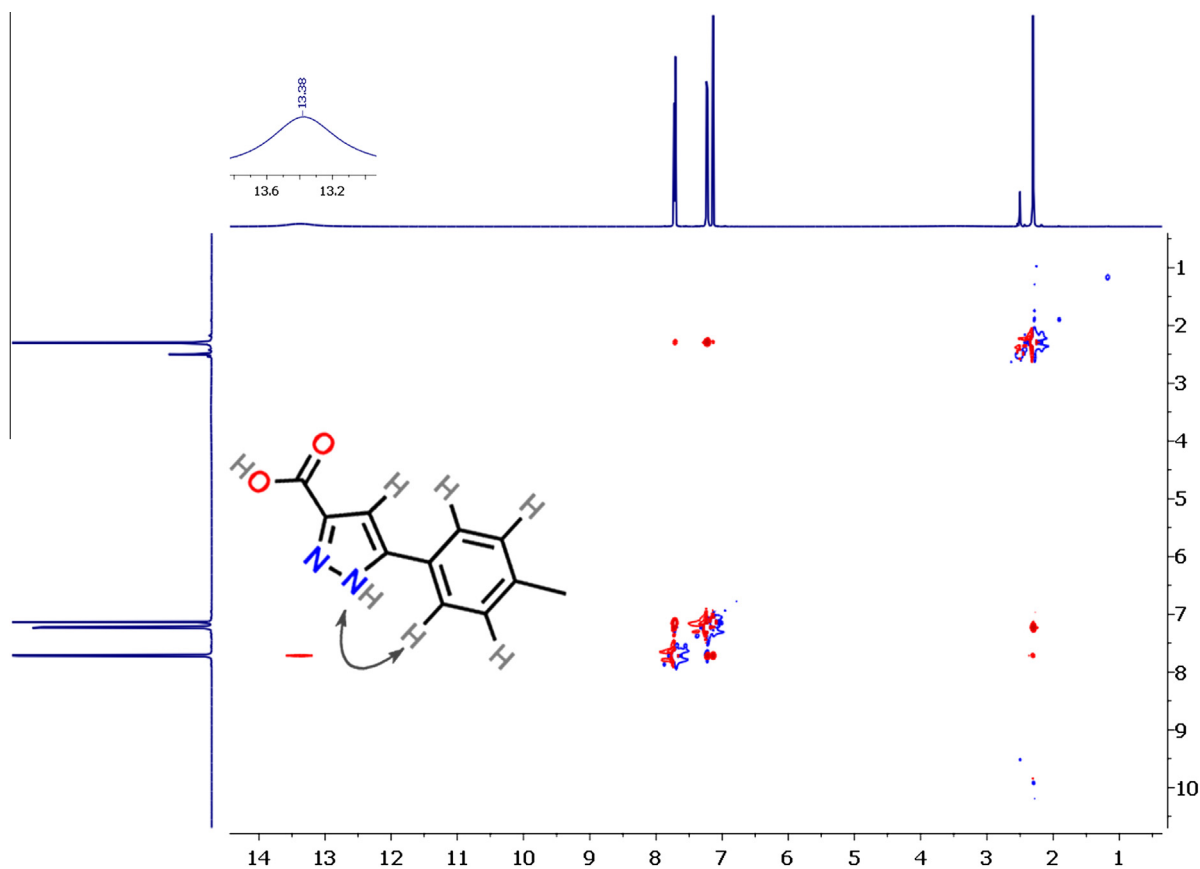


Figure 1. NOESY spectrum of 4-Me-derivative (1) in DMSO. Signal between *ortho*-Ph-hydrogens and pyrazole NH is illustrated.

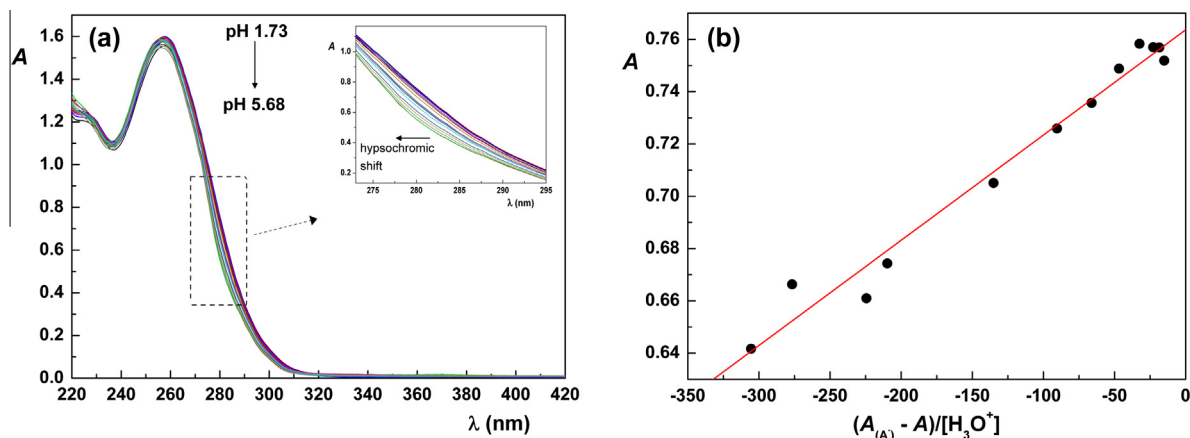


Figure 2. (a) UV/Vis Spectra of compound **22** in pH range 1.73–5.68 used for pK_{a1} determination ($t = 25 \pm 1$ °C); wavelength range used for calculations is magnified; (b) Determination of K_{a1} at 280 nm according to Eq. 1; slope = $4.0 \pm 0.2 \times 10^{-4}$, intercept = 0.764 ± 0.003 , $r^2 = 0.973$.

Table 1

Structures of compounds **1–23** and inhibitory activities (given as K_i) toward four CA isoforms

| Compound | R- | K_i^+ (μM) | | | |
|--------------|--------------------------|---------------------------|--------|--------|---------|
| | | hCA I | hCA II | hCA IX | hCA XII |
| 1 | 4-Me- | >50 | >50 | >50 | >50 |
| 2 | 4-Et- | >50 | >50 | 42 | 4.5 |
| 3 | 4- <i>i</i> -Pr- | >50 | >50 | >50 | >50 |
| 4 | 4- <i>n</i> -Bu- | >50 | >50 | 39 | 5.5 |
| 5 | 4- <i>t</i> -Bu- | >50 | >50 | 5 | 21 |
| 6 | 2,4-di-Me- | >50 | >50 | 45 | >50 |
| 7 | 3,4-di-Me- | >50 | >50 | 48 | >50 |
| 8 | 2,4,5-tri-Me- | >50 | >50 | 23.5 | >50 |
| 9 | 2,3,5,6-tetra-Me- | >50 | >50 | 5 | >50 |
| 10 | 2,4,6-tri-Et- | >50 | >50 | >50 | >50 |
| 11 | 2,4-di- <i>i</i> -Pr- | >50 | >50 | 16 | >50 |
| 12 | 2,4,6-tri- <i>i</i> -Pr- | >50 | >50 | 39 | 39 |
| 13 | β -Tetralinyl- | >50 | >50 | >50 | 43.5 |
| 14 | β -Naphthyl- | >50 | >50 | >50 | 5.5 |
| 15 | 4-Ph- | >50 | >50 | >50 | 4 |
| 16 | 4-Pyrrolidine- | >50 | >50 | >50 | 33.5 |
| 17 | 4-F- | >50 | >50 | >50 | 38.5 |
| 18 | 4-Cl- | >50 | >50 | >50 | 50 |
| 19 | 3-Br- | >50 | >50 | 23.5 | >50 |
| 20 | 4-OH- | >50 | >50 | >50 | 41 |
| 21 | 2-OMe- | >50 | >50 | >50 | 50 |
| 22 | 4-OMe- | >50 | >50 | 49.5 | >50 |
| 23 | 4-OMe-2,5-di-Me- | >50 | >50 | 22.5 | >50 |
| AAZ** | / | 0.25 | 0.012 | 0.025 | 0.006 |

* Mean from three different assays, errors in the range of 5–10% of the reported values (data not shown).

** Acetazolamide (5-acetamido-1,3,4-thiadiazole-2-sulfonamide, **AAZ**) was used as a standard inhibitor.

of the water was estimated from PDB entry 4E3G,¹³ *para*-hydroxybenzoic acid co-crystallized with CA II, and further refined by the WaterFLAP protocol. All compounds were treated in their anionic forms, with deprotonated carboxyl group, in accordance with predicted and experimentally determined pK_a values. Both tautomers A and B, **Scheme 2**, were used for docking. Initial attempts of docking compounds into the active site of each isoform appeared very inconclusive, so we proceeded considering the whole enzyme as a target.

The docking study found all compounds bound out of the active site of CA I (**Fig. S4 in Supplementary Material**), in the cleft lined by the residues Pro13, Asn24, Thr100 and His103. The carboxylate

anion of these compounds makes polar interactions with Ser99 and Thr100 hydroxyl groups, while the pyrazole nitrogens make polar interactions with Asn245 side-chain and His103 backbone carbonyl. Larger alkyl substituents were typically anchored between side chains of Pro13 and Pro247. For CA II, the docking study also found majority of the compounds out of the active site (**Fig. S5 in Supplementary Material**). The compounds are clustered in a region lined with residues: Trp5, Lys170, Asn232 and Pro237. The carboxylate anion makes polar interactions with His4 NH backbone and Lys170 side chain NH_3^+ , whereas the pyrazole NH was hydrogen bonded with Phe231 backbone carbonyl. For CA I and CA II similar docking solutions were found irrespective of the position of the His64 ('in' or 'out').

Such results revealed higher affinity of these compounds toward regions of CA I and CA II out of enzyme active site and can offer possible explanation of inactivity of **1–23** toward these cytosolic CA isoforms studied here.

Our docking study found all compounds bound close to the active site Zn^{2+} ion of CA IX and CA XII (including those for which $K_i > 50$ μM were measured). All compounds were clustered with very similar orientation of the pyrazole-COO⁻ moiety in the active site of each isoform, but orientation of this part of the molecule appears different in CA IX and CA XII, respectively. In CA IX, the carboxylate anion makes polar interactions with the hydroxyl group of Thr199 and Thr200 and with the water coordinated to zinc. The pyrazole NH makes polar interactions with Gln67 side-chain carbonyl. As a trend, compounds found as active toward CA IX (**Table 1**) have alkyl substituents in *ortho*- and *meta*-positions of the phenyl ring. Compounds having bulkier substituents in *para*-position appeared to be inactive. Visual inspection of docking results revealed that *ortho*- and *meta*-substituted compounds, as well as those having medium-sized alkyl substituents in *para*-position assessed better shape complementarity with the cleft of active site than the rest of the investigated compounds, which were inactive toward CA IX. This cleft is lined by backbone of residues Trp5, Asn62 and His64, and situated distal from the sequence 131–134. (**Fig. 3** and **Fig. S6 in Supplementary Material**). These residues were shown earlier to be involved in the binding of various classes of CAIs or CA activators.²⁴

This observation could explain the structural features that differentiate active from inactive compounds towards CA IX. Along with this, we observed that compounds **9** (2,3,5,6-tetra-methyl derivative) and **5** (4-*t*-butyl derivative) with $K_i < 10$ μM , have mutually very similar 3D-dependent whole-molecular properties, particularly apolar surface area and volume (**Table S2 in Supplementary Material**).

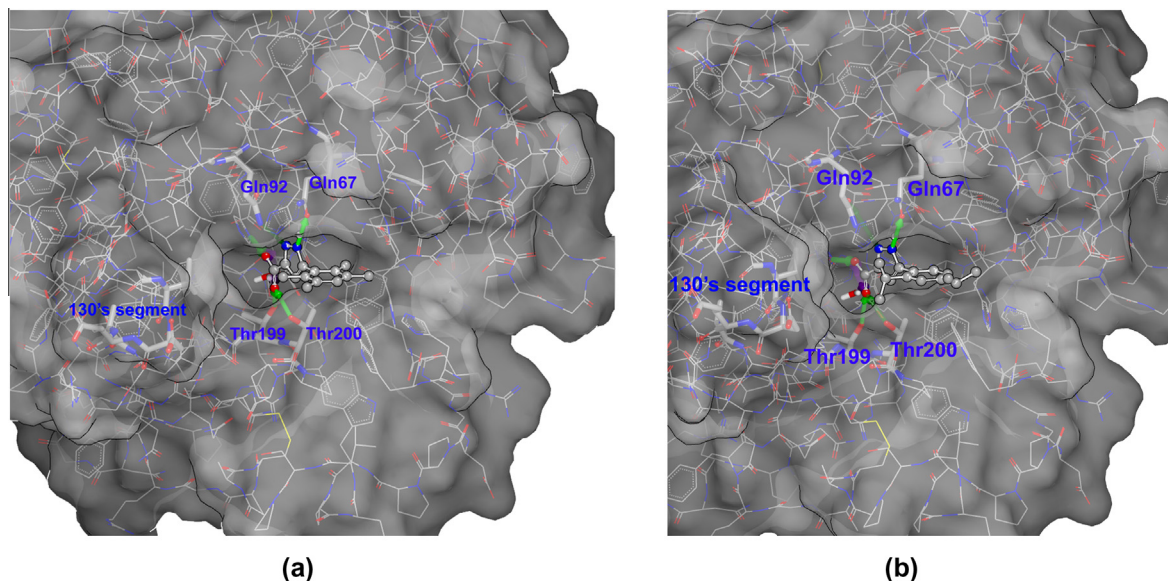


Figure 3. Best-ranked solutions of compounds **9** (a) and **11** (b) docked into CAIX.

Docking solutions for CA XII found all compounds close to the active site Zn^{2+} ion, but in orientations quite different compared to CA IX. The carboxylate anion makes polar interactions with Tyr7 and Thr199 hydroxyl groups, or Asn62 side-chain NH_2 . The pyrazole NH and N make polar interactions with Asn62 side-chain or water-mediated interactions with the Thr199. Aromatic moiety of the compounds were directed toward the sequence 131–134 (130's segment). This part of the active site is specific for CA XII and it was suggested that can be used for the design of isoform specific inhibitors.²³ Visual inspection of the docking results showed that aryl moiety of all compounds found active towards CA XII makes van-der Waals contacts with the 130's segment, while the same moiety in inactive compounds cannot reach this segment (Fig. 4 and Fig. S7 in Supplementary Material). This rationalizes the structure-activity relationship data of **1–23** observed towards CA XII and shown in Table 1.

It should be noted that we did not observe any regularity between calculated affinities of compounds (docking scores) and

the order of activity toward CA IX or CA XII. ChemGauss4 scoring function accounts for shape and electrostatic complementarities, as well as the binding site and the ligand desolvation penalty. Not overall scoring, nor shape complementarities show any trend with the experimentally found K_i values. Considering the wide and conical shape of the CA active site, the congeneric set of examined compounds—different in apolar moieties only, and the narrow range of K_i values, such an observation is not surprising.

In literature, we found one systematic comparison of CAs I, II, IX and XII active sites.²⁵ CA active site residues involved in ligand binding were listed and similarity and differences commented. In order to elucidate more structural information that can explain selectivity of **1–23** toward membrane-associated isoforms, we studied active sites of CA I, II, IX and XII by GRID force field.²⁶ Molecular interaction fields (MIFs) were calculated by hydrophobic (DRY), HBD (N1) and HBA (O) probes in the box encompassing active site residues that interact with small molecules in so far reported crystal structures of CAs (for details see Section 4 and

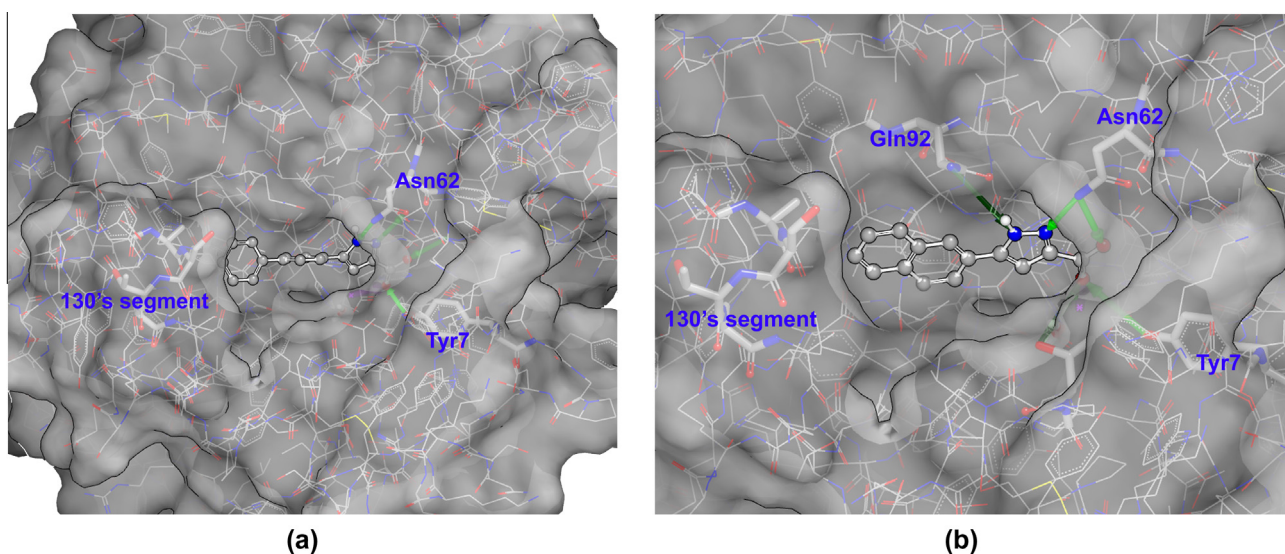


Figure 4. Best-ranked solutions of compounds **15** (a) and **14** (b) docked into CAXII.

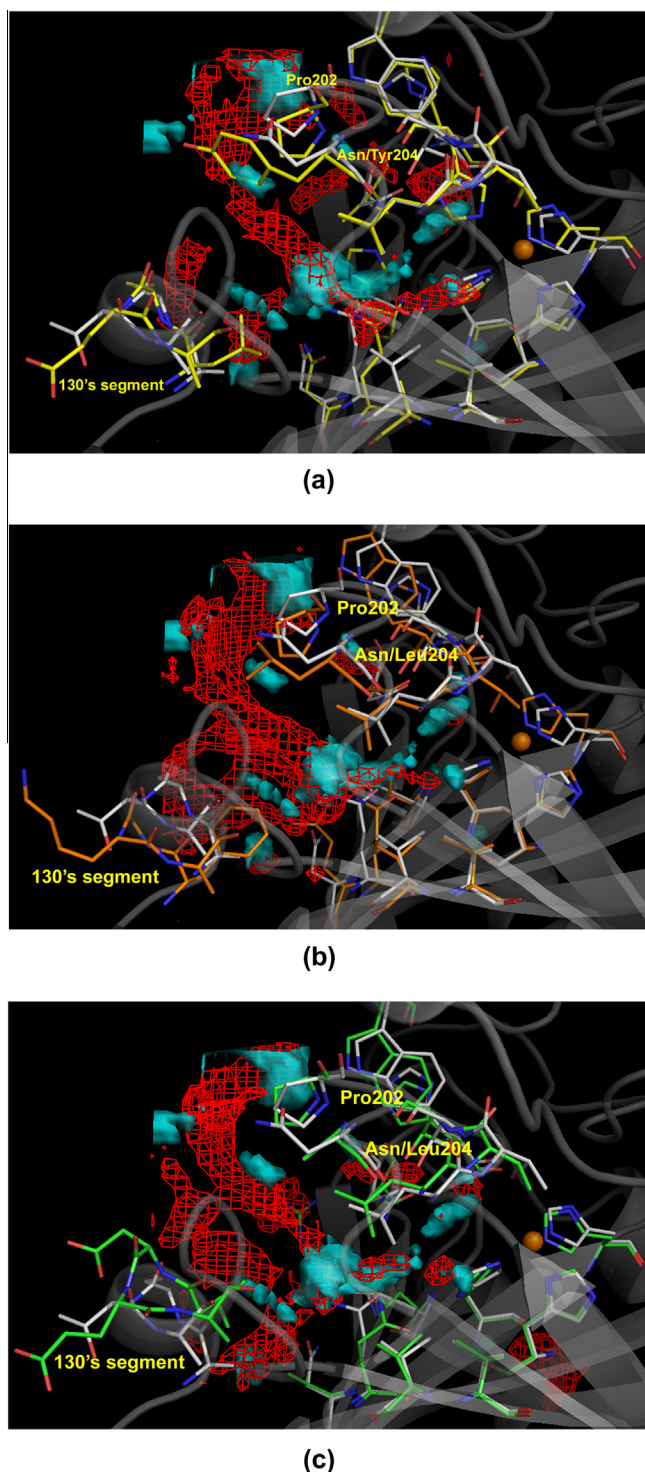


Figure 5. Isosurface of DRY molecular-interaction field in the active site of CAI, II, IX and XII, depicted on -0.7 kcal/mol. (a) Comparison between CAXII (blue solid field, grey sticks) and CAI (red mesh field, yellow sticks). (b) Comparison between CAXII (blue solid field, grey sticks) and CAII (red mesh field, orange sticks). (c) Comparison between CAXII (blue solid field, grey sticks) and CAIX (red mesh field, green sticks). Pro202, conserved in the each CA isoform studied, and residues in position 204 are labeled. Among other residues shown, residues of 130's segment (residues 131–134) on the left side and His residues which coordinates active site Zn²⁺ ion (94, 96 and 119) on the right side are given in stick presentation, without explicit labels; while active site Zn²⁺ ion is given as the orange sphere.

the [Supplementary Material, file 2](#)). Inspection of the results revealed expected differences of MIFs obtained with HBA and HBD probe (O and N1) in vicinity of residue 67 ([Fig. S8 in](#)

[Supplementary Material](#)). In this position mutually similar Asn of CA II or Gln of CA IX are replaced with His in CA I or Lys in CA XII. Less obvious difference appears by comparison of MIFs obtained by hydrophobic probe (DRY). In all four isoforms studied here, the global minimum of DRY probe, on about -3 kcal/mol, appears in vicinity of Pro202—conserved in all four enzymes. On arbitrary chosen isocontour level of -0.7 to -0.9 kcal/mol, we observed 'continuous' isosurface of DRY probe from the region of Pro202 to the region between Leu198 and Gln92 in CAs I, II and IX, [Figure 5](#).

In CA XII, DRY isosurface appears only in region of Pro202 and region between Leu198 and Gln92, but those two isosurface are not mutually connected ([Fig. 5](#)). Such a difference appears not only because significantly less voluminous, apolar Ala131 in CA XII, compared with Leu in CA I, Phe in CA II and Val in CA IX in this position; but also because of differences of residue in position 204, situated between Pro200 and Leu198. In CA I this is Ala, in CA II Leu, and in CA IX Tyr. All three residues can form hydrophobic interactions. In CA XII, the residue in position 204 is Asn that can make preferably polar interactions. To the best of our knowledge such differences among the four CA isoforms studied in this work were not explicitly described in literature so far, and can be used for design of isoform selective inhibitors by introduction of suitable hydrophobic/hydrophilic moiety relatively far from the ZBG. Probably because of feasibility of CA II crystallization, there are significantly less wild-type CA XII crystal structures comparing with CA II, or mimics of other isoforms derived by targeted mutations of CA II. Thus, in the literature so far, mainly differences in the 130's segment have been exploited for the design of CA XII selective inhibitors.

From our docking solutions of the four most potent derivatives toward CA XII (compounds **2**, **4**, **14**, **15**), we observed that their phenyl moieties fairly fit to DRY minima between Leu198 and Gln92 ([Fig. 6](#)), while the same moieties of inactive derivatives are displaced from this region.

Considering the activity of these compounds against CA IX and XII, the results obtained by our docking study and comparison of the four isoforms active sites suggested that more flexibility imposed to novel congeners will be desirable for increasing inhibitory potency, whereas bulkiness of phenyl substituents should be retained in order to have isoform selectivity toward CA XII. Having two rotatable bonds in the core structure (Ph-pyrazole-COOH), and substituents on the phenyl ring with the very limited conformational freedom (except in the 4-*n*-Bu derivative, **4**), our compounds appeared relatively rigid. Thus, anchored near the Zn-bound water by the $-\text{COO}^-$ moiety, their hydrophobic moieties cannot simultaneously reach parts of the active site relatively far from the Zn²⁺ ion to make stronger non-covalent interactions. These conclusions may be useful for the design of novel congeners of CAIs incorporating carboxylate ZBGs.

3. Conclusions

We described the synthesis and inhibitory activity of a congeneric set of 23 phenyl-substituted 5-phenyl-1*H*-pyrazole-3-carboxylic acids toward human CA isoforms I, II, IX and XII. The compounds were active in 4–50 μM range and showed strong preferences toward CA IX and XII over CA I and II. Due to such a selectivity, 5-aryl-pyrazole-3-carboxylic acids reported in this work could be used for further development of isoform-specific inhibitors. The results of our docking study offered possible explanations on the selectivity of these compounds toward CA IX and XII, as well as on their diverse affinity depending on the substitution pattern of the aryl moiety. Comparison of active sites of all four isoforms studied by GRID generated molecular-interaction fields revealed interesting differences between CA XII and other three isoforms

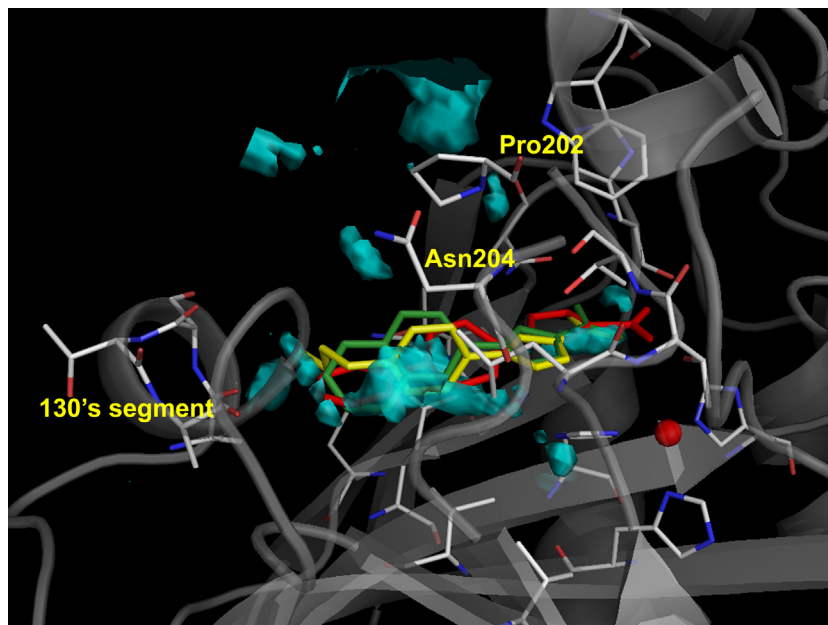


Figure 6. Best-ranked docking solutions for compounds **4** (yellow sticks), **14** (green sticks) and **15** (red sticks) overlapped with the isosurface of DRY probe (-0.7 kcal/mol) in the CA XII active site. Pro202 and Asn204, given in stick presentation, are labeled. Among other residues shown, residues of 130's segment (residues 131–134) on the left side and His residues which coordinates active site Zn^{2+} ion (94, 96 and 119) on the right side are given in stick presentation, without explicit labels; while active site Zn^{2+} ion is given as a red sphere.

in regions that have high affinity towards hydrophobic moieties. To the best of our knowledge such an observation was not reported so far and can foster development of the selective CA XII inhibitors.

4. Experimental

4.1. Chemistry

All chemicals were purchased from Fluka, Aldrich, or Merck, having >98% purity, and were used as received. For the thin-layer chromatography, silica gel pre-coated plates with fluorescent indicator (254 nm) were used. Melting points were determined in open capillary tubes on Stuart SMP-10 apparatus and are uncorrected. ESI-MS (Electrospray ionization mass spectrometry) analysis was performed in methanol on an Agilent Technologies 6210-1210 TOF-LC-ESI-MS instrument in positive mode. IR (Infra-red) spectra were recorded on a Thermo Nicolet 6700 FT-IC spectrophotometer, by ATR (Attenuated total reflectance). 1H , ^{13}C NMR (Nuclear magnetic resonance) and NOESY (Nuclear Overhauser effect spectroscopy) spectra were recorded in $DMSO-d_6$ on Bruker AVANCE 500/125 MHz or on a Varian Gemini2000 200/50 MHz instruments. Chemical shifts are reported in parts per million (ppm) relative to tetramethylsilane (TMS) and spin multiplicities are given as follows: s (singlet), d (doublet), t (triplet), q (quartet), qn (quintet), sx (sextet), h (heptet) m (multiplet), br (broad). UV/Vis Spectra were recorded on Thermo Scientific Evolution 60S spectrophotometer (Thermo Fisher Scientific Inc, Waltham, Massachusetts, USA). pH Values were measured using CRISON pH-Burette 24 2S equipped with CRISON 50 29 micro-combined pH electrode (Crison Instruments, S.A. Spain). The electrode was calibrated by standard CRISON buffer solutions (pH 4.01, 7.00, and 9.21).

4.1.1. Typical experimental procedure for synthesis of 1–23

4.1.1.1. 5-(4-Methylphenyl)-1H-pyrazole-3-carboxylic acid (1). 0.4 g of 4-(4-methylphenyl)-2,4-dioxobutanoic acid was dissolved in 20 ml of glacial acetic acid in 50 ml round-bottom flask. In a stirred solution, 280 μ L (3 eq.) of hydrazine monohydrate

($N_2H_4 \cdot H_2O$) was added dropwise. The color of solution was changed to pale yellow immediately after addition of first amount of hydrazine. The progress of reaction was monitored by TLC. After completion, reaction mixture was poured in 50 ml H_2O and left to stir overnight. White precipitate was collected, dried on air and recrystallized from the mixture of hexane/EtOH (\sim 9:1), giving 0.34 g of product (87% of theoretical yield).

4.1.2. Characterization of compounds 1–23

4.1.2.1. 5-(4-Methylphenyl)-1H-pyrazole-3-carboxylic acid (1). White solid; mp = 253–254 $^{\circ}C$ (hexane/EtOH); $C_{11}H_{10}N_2O_2$, $M_w = 202.21$; ESI-MS: Calculated for $C_{11}H_{11}N_2O_2$ $[M+H]^+$: 203.08150, measured: 203.08063; IR (ν , cm^{-1}): 3264 (N–H), 1696 (C=O), 1500, 1198; 1H NMR (500 MHz, $DMSO-d_6$) δ (ppm): 2.30 (s, 3 H), 7.14 (s, 1 H), 7.22 (d, $J = 7.83$ Hz, 2 H), 7.71 (d, $J = 8.31$ Hz, 2 H), 13.38 (br). ^{13}C NMR (125 MHz, $DMSO-d_6$) δ (ppm): 20.85, 104.91, 125.25, 128.13, 129.48, 137.58, 140.09, 147.44, 162.04.

4.1.2.2. 5-(4-Ethylphenyl)-1H-pyrazole-3-carboxylic acid (2). Starting from 0.625 g of 4-(4-ethylphenyl)-2,4-dioxobutanoic acid, 0.55 g of product was obtained (89% of theoretical yield). White solid; mp = 229–230 $^{\circ}C$ (hexane/EtOH); $C_{12}H_{12}N_2O_2$, $M_w = 216.24$; ESI-MS: Calculated for $C_{12}H_{13}N_2O_2$ $[M+H]^+$: 217.09715, measured: 217.09634; IR (ν , cm^{-1}): 3265 (N–H), 1692 (C=O), 1498, 1237; 1H NMR (200 MHz, $DMSO-d_6$) δ (ppm): 1.17 (t, $J = 7.30$ Hz, 3 H), 2.60 (q, $J = 7.30$ Hz, 2 H), 7.14 (s, 1 H), 7.26 (d, $J = 7.86$ Hz, 2 H), 7.74 (d, $J = 8.42$ Hz, 2 H), 12.93 (br); ^{13}C NMR (50 MHz, $DMSO-d_6$) δ (ppm): 15.74, 28.19, 105.19, 125.60, 128.57, 140.48, 144.19, 147.67, 162.32.

4.1.2.3. 5-(4-Isopropylphenyl)-1H-pyrazole-3-carboxylic acid (3). Starting from 0.095 g of 4-(4-isopropylphenyl)-2,4-dioxobutanoic acid, 0.078 g of product was obtained (83% of theoretical yield). White solid; mp = 241–243 $^{\circ}C$ (hexane/EtOH); $C_{13}H_{14}N_2O_2$, $M_w = 230.26$; ESI-MS: Calculated for $C_{13}H_{15}N_2O_2$ $[M+H]^+$: 231.11280, measured: 231.11197. IR (ν , cm^{-1}): 3229 (N–H), 1691

(C=O), 1499, 1194; ^1H NMR (200 MHz, DMSO- d_6) δ (ppm): 1.22 (d, $J = 6.74$ Hz, 6 H) 2.91 (h, $J = 6.74$ Hz, 1 H) 7.14 (s, 1 H) 7.31 (d, $J = 7.86$ Hz, 2 H) 7.76 (d, $J = 8.42$ Hz, 2 H) 13.05 (br). ^{13}C NMR (50 MHz, DMSO- d_6) δ (ppm): 23.99, 33.43, 105.11, 125.58, 127.05, 128.78, 148.70, 162.27.

4.1.2.4. 5-(4-*n*-Butylphenyl)-1*H*-pyrazole-3-carboxylic acid (4). Starting from 0.52 g of 4-(4-*n*-butylphenyl)-2,4-dioxobutanoic acid, 0.435 g of product was obtained (85% of theoretical yield). White solid; mp = 203–205 °C, dec. (hexane/EtOH); $\text{C}_{14}\text{H}_{16}\text{N}_2\text{O}_2$, $M_w = 244.29$; ESI-MS: Calculated for $\text{C}_{14}\text{H}_{17}\text{N}_2\text{O}_2$ $[\text{M}+\text{H}]^+$: 245.12845, measured: 245.12744; IR (ν , cm^{-1}): 3320 (N–H), 1665 (C=O), 1455, 1265; ^1H NMR (200 MHz, DMSO- d_6) δ (ppm): 0.85 (t, $J = 7.30$ Hz, 3 H), 1.26 (sx, $J_{1,2} = 7.30$ Hz, 2 H), 1.52 (qn, $J = 7.30$ Hz, 2 H), 2.55 (t, $J = 7.30$ Hz, 2 H), 7.14 (s, 1 H), 7.22 (d, $J = 8.42$ Hz, 2 H), 7.73 (d, $J = 7.86$ Hz, 2 H), 13.09 (br); ^{13}C NMR (50 MHz, DMSO- d_6) δ (ppm): 14.03, 22.02, 33.31, 34.87, 105.19, 125.54, 128.62, 129.09, 138.12, 142.77, 147.79, 162.38.

4.1.2.5. 5-(4-*tert*-Butylphenyl)-1*H*-pyrazole-3-carboxylic acid (5). Starting from 0.62 g of 4-(4-*tert*-butylphenyl)-2,4-dioxobutanoic acid, 0.48 g of product was obtained (79% of theoretical yield). White solid; mp = 257–259 °C, dec. (hexane/EtOH); $\text{C}_{14}\text{H}_{16}\text{N}_2\text{O}_2$, $M_w = 244.29$; IR (ν , cm^{-1}): 3315 (N–H), 3145, 1723 (C=O), 1584, 1210; ESI-MS: Calculated for $\text{C}_{14}\text{H}_{17}\text{N}_2\text{O}_2$ $[\text{M}+\text{H}]^+$: 245.12845, measured: 245.12888; ^1H NMR (200 MHz, DMSO- d_6) δ (ppm): 2.50 (s, 9 H, overlapped with the solvent signal), 8.31 (s, 1 H), 8.65 (d, $J = 7.86$ Hz, 2 H), 8.98 (d, $J = 7.86$ Hz, 2 H), 9.94 (br); ^{13}C NMR (50 MHz, DMSO- d_6) δ (ppm): 31.29, 34.56, 104.70, 125.29, 125.82, 129.20, 141.27, 148.25, 150.65, 162.78.

4.1.2.6. 5-(2,4-di-Methylphenyl)-1*H*-pyrazole-3-carboxylic acid (6). Starting from 0.58 g of 4-(2,4-di-methylphenyl)-2,4-dioxobutanoic acid, 0.49 g of product was obtained (86% of theoretical yield). White solid, mp = 248–249 °C (hexane/EtOH); $\text{C}_{12}\text{H}_{12}\text{N}_2\text{O}_2$, $M_w = 216.24$; ESI-MS: Calculated for $\text{C}_{12}\text{H}_{13}\text{N}_2\text{O}_2$ $[\text{M}+\text{H}]^+$: 217.09715, measured: 217.09704; IR (ν , cm^{-1}): 3099 (N–H, overlapped with C–H), 2975, 2917, 1695 (C=O), 1494, 1423, 1279; ^1H NMR (200 MHz, DMSO- d_6) δ (ppm): 3.51 (s, 3 H), 3.58 (s, 3 H), 8.11 (s, 1 H), 8.24–8.36 (m, 3 H; overlapped *ortho*-H doublet with *meta*-H signals (doublet and splitted singlet)), 8.62 (d, $J = 7.86$ Hz, 4 H), 14.29 (br). ^{13}C NMR (50 MHz, DMSO- d_6) δ (ppm): 20.93, 108.01, 126.94, 127.78, 129.08, 131.79, 135.56, 137.89, 140.56, 146.72, 162.69.

4.1.2.7. 5-(3,4-di-Methylphenyl)-1*H*-pyrazole-3-carboxylic acid (7). Starting from 0.38 g of 4-(3,4-di-methyl phenyl)-2,4-dioxobutanoic acid, 0.33 g of product was obtained (88% of theoretical yield). White solid, mp = 276–277 °C (hexane/EtOH); $\text{C}_{12}\text{H}_{12}\text{N}_2\text{O}_2$, $M_w = 216.24$; ESI-MS: Calculated for $\text{C}_{12}\text{H}_{13}\text{N}_2\text{O}_2$ $[\text{M}+\text{H}]^+$: 217.09715, measured: 217.09685; IR (ν , cm^{-1}): 3107 (N–H, C–H), 2917, 1697 (C=O), 1508, 1469, 1270; ^1H NMR (200 MHz, DMSO- d_6) δ (ppm): 2.24 (s, 3 H), 2.27 (s, 3 H), 7.15 (s, 1 H), 7.20 (d, $J = 7.86$ Hz, 1 H), 7.57 (d, $J = 7.86$ Hz, 1 H), 7.65 (s, 1 H), 13.38 (br); ^{13}C NMR (50 MHz, DMSO- d_6) δ (ppm): 19.43, 19.71, 105.08, 122.99, 126.67, 128.58, 130.22, 136.63, 137.01, 140.60, 147.62, 162.45.

4.1.2.8. 5-(2,4,5-tri-Methylphenyl)-1*H*-pyrazole-3-carboxylic acid (8). Starting from 0.35 g of 4-(2,4,5-tri-methylphenyl)-2,4-dioxobutanoic acid, 0.28 g of product was obtained (81% of theoretical yield). White solid, mp = 227–228 °C (hexane/EtOH); $\text{C}_{13}\text{H}_{14}\text{N}_2\text{O}_2$, $M_w = 230.26$; ESI-MS: Calculated for $\text{C}_{13}\text{H}_{15}\text{N}_2\text{O}_2$ $[\text{M}+\text{H}]^+$: 231.11280, measured: 231.11234; IR (ν , cm^{-1}): 3163, 3109 (N–H, overlapped with C–H), 1696 (C=O), 1514, 1277. ^1H NMR (200 MHz, DMSO- d_6) δ (ppm): 2.22 (s, 6 H), 2.33 (s, 3 H),

3.91 (pyrazole CH_2 of tautomer C (Scheme 2)), ~34% in respect to main tautomer), 6.88 (s, 1 H), 7.07 (s, 1 H), 7.31 (s, 1 H), 13.33 (br); ^{13}C NMR (50 MHz, DMSO- d_6) δ (ppm): 19.20, 20.40, 51.64 (pyrazole CH_2 of tautomer C (Scheme 2)), 107.86, 127.80, 130.11, 132.32, 132.73, 133.90, 136.56, 140.69, 146.57, 162.72.

4.1.2.9. 5-(2,3,5,6-tetra-Methylphenyl)-1*H*-pyrazole-3-carboxylic acid (9). Starting from 0.37 g of 4-(2,3,5,6-tetra-methylphenyl)-2,4-dioxobutanoic acid, 0.33 g of product was obtained (91% of theoretical yield). White solid, mp = 246–248 °C, dec. (hexane/AcOEt); $\text{C}_{14}\text{H}_{16}\text{N}_2\text{O}_2$, $M_w = 244.29$; ESI-MS: Calculated for $\text{C}_{14}\text{H}_{17}\text{N}_2\text{O}_2$ $[\text{M}+\text{H}]^+$: 245.12845, measured: 245.12844; IR (ν , cm^{-1}): 3244 (N–H), 3123, 2927, 1718 (C=O), 1471, 1410, 1242; ^1H NMR (500 MHz, DMSO- d_6) δ (ppm): 1.88 (s, 6 H), 2.20 (s, 6 H), 6.57 (s, 1 H), 7.05 (s, 1 H), 13.06 (br). ^{13}C NMR (125 MHz, DMSO- d_6) δ (ppm): 16.66, 19.69, 108.14, 130.47, 131.65, 133.19, 142.40, 144.52, 163.03.

4.1.2.10. 5-(2,4,6-tri-Ethylphenyl)-1*H*-pyrazole-3-carboxylic acid (10). Starting from 0.41 g of 4-(2,4,6-tri-ethylphenyl)-2,4-dioxobutanoic acid, 0.33 g of product was obtained (82% of theoretical yield). White solid, mp = 221–224 °C, dec. (hexane/AcOEt); $\text{C}_{16}\text{H}_{20}\text{N}_2\text{O}_2$, $M_w = 272.34$; ESI-MS: Calculated for $\text{C}_{16}\text{H}_{21}\text{N}_2\text{O}_2$ $[\text{M}+\text{H}]^+$: 273.15975, measured: 273.15938; IR (ν , cm^{-1}): 3145 (N–H, broad), 2967, 1712 (C=O), 1460, 1263; ^1H NMR (200 MHz, DMSO- d_6) δ (ppm): 0.98 (t, $J = 7.30$ Hz, 6 H), 1.20 (t, $J = 7.30$ Hz, 4 H), 2.30 (q, $J_{1,2} = 7.30$ Hz, 4 H), 2.60 (q, $J = 7.30$ Hz, 2 H) 6.65 (s, 1 H) 7.00 (s, 2 H) 13.07 (br); ^{13}C NMR (50 MHz, DMSO- d_6) δ (ppm): 15.88, 16.01, 26.63, 28.37, 108.77, 125.56, 126.84, 143.48, 143.90, 144.97, 163.23.

4.1.2.11. 5-(2,4-di-Isopropylphenyl)-1*H*-pyrazole-3-carboxylic acid (11). Starting from 0.35 g of 4-(2,4-di-isopropylphenyl)-2,4-dioxobutanoic acid, 0.28 g of product was obtained (79% of theoretical yield). White solid, mp = 213–216 °C, dec. (hexane/AcOEt); $\text{C}_{16}\text{H}_{20}\text{N}_2\text{O}_2$, $M_w = 272.34$; ESI-MS: Calculated for $\text{C}_{16}\text{H}_{21}\text{N}_2\text{O}_2$ $[\text{M}+\text{H}]^+$: 273.15975, measured: 273.15940; IR (ν , cm^{-1}): 3232 (N–H), 2962, 1704 (C=O), 1465, 1273; ^1H NMR (200 MHz, DMSO- d_6) δ (ppm): 1.16 (d, $J = 6.74$ Hz, 6 H), 1.22 (d, $J = 6.74$ Hz, 6 H), 2.91 (h, $J = 6.74$ Hz, 1 H), 3.20 (h, $J = 6.74$ Hz, 1 H), 6.75 (s, 1 H), 7.12 (d, splitted $J_{1,2} = 1.68$ Hz, $J_{1,3} = 7.86$ Hz, 1 H), 7.25 (d, b, $J = 7.86$ Hz, 1 H), overlapped with 7.28 (s, 1H), 13.26 (br); ^{13}C NMR (50 MHz, DMSO- d_6) δ (ppm): 29.28, 33.74, 108.21, 123.74, 123.96, 127.55, 130.17, 146.99, 149.43, 162.70

4.1.2.12. 5-(2,4,6-tri-Isopropylphenyl)-1*H*-pyrazole-3-carboxylic acid (12). Starting from 0.32 g of 4-(2,4,6-tri-isopropylphenyl)-2,4-dioxobutanoic acid, 0.21 g of product was obtained (66% of theoretical yield). ESI-MS: Pale yellow solid, mp = 217–219 °C, dec. (hexane/AcOEt); $\text{C}_{19}\text{H}_{26}\text{N}_2\text{O}_2$, $M_w = 314.42$; Calculated for $\text{C}_{19}\text{H}_{27}\text{N}_2\text{O}_2$ $[\text{M}+\text{H}]^+$: 315.20670, measured: 315.20693; IR (ν , cm^{-1}): 3154 (N–H, C–H), 2961, 1700 (C=O), 1567, 1461; ^1H NMR (200 MHz, DMSO- d_6) δ (ppm): 1.08 (d, $J = 6.74$ Hz, 12H), 1.24 (d, $J = 6.74$ Hz, 6 H), 2.49 (h, $J = 6.74$ Hz, 1H, overlapped with DMSO- d_6 signal), 2.92 (h, $J = 6.74$ Hz, 1H), 3.82 (pyrazole CH_2 of tautomer C (Scheme 2)), ~36% in respect to main tautomer), 6.65 (s, 1H), 7.10 (s, 2H), 13.09 (br, 2H); ^{13}C NMR (50 MHz, DMSO- d_6) δ (ppm): 23.98, 30.20, 33.83, 51.53 (pyrazole CH_2 of tautomer C (Scheme 2)), 108.83, 120.40, 125.49, 148.16, 149.63, 163.13.

4.1.2.13. 5-(5,6,7,8-Tetrahydronaphthalen-2-yl)-1*H*-pyrazole-3-carboxylic acid (13). Starting from 0.51 g of 4-(5,6,7,8-tetrahydronaphthalen-2-yl)-2,4-dioxobutanoic acid, 0.41 g of product was obtained (82% of theoretical yield). White solid, mp = 234–236, dec. (hexane/EtOH); $\text{C}_{14}\text{H}_{14}\text{N}_2\text{O}_2$, $M_w = 242.27$; ESI-MS: Calculated for $\text{C}_{14}\text{H}_{15}\text{N}_2\text{O}_2$ $[\text{M}+\text{H}]^+$: 243.11280, measured:

243.11257; IR (ν , cm^{-1}): 3104 (N–H, broad), 2925, 1697 (C=O), 1430, 1270; ^1H NMR (500 MHz, DMSO- d_6) δ (ppm): 1.72 (m, b, 4 H) 2.70 (s, b, 2 H), 2.74 (s, b, 2H) 7.07–7.09 (m, overlapped pyrazole CH singlet and *meta*-H doublet, 2 H) 7.50–7.52 (m, overlapped *ortho*-Hs singlet and doublet, 2 H), 13.32 (br); ^{13}C NMR (125 MHz, DMSO- d_6) δ (ppm): 22.71, 28.63, 28.87, 104.77, 122.54, 125.75, 127.95, 129.42, 136.82, 137.11, 140.38, 147.35, 162.12.

4.1.2.14. 5-(Naphthalen-2-yl)-1H-pyrazole-3-carboxylic acid (14). Starting from 0.58 g of 4-(naphthalen-2-yl)-2,4-dioxobutanoic acid, 0.49 g of product was obtained (82% of theoretical yield). White solid, mp = 274–276 °C, dec. (hexane/AcOEt); $\text{C}_{14}\text{H}_{10}\text{N}_2\text{O}_2$, $M_w = 238.24$; ESI-MS: Calculated for $\text{C}_{14}\text{H}_{11}\text{N}_2\text{O}_2$ $[\text{M}+\text{H}]^+$: 239.08150, measured: 239.08065; IR (ν , cm^{-1}): 3206 (N–H), 1683 (C=O), 1501, 1274; ^1H NMR (200 MHz, DMSO- d_6) δ (ppm): 7.23 (s, 1 H), 7.50 (t, $J_{1,2} = 3.93$ Hz, 2 H), 7.89 (d, overlapped with doublet at 7.95, 1 H), 7.95 (d, $J = 8.42$ Hz, 2 H), 8.04 (d, $J = 8.42$ Hz, 1 H), 8.39 (s, 1 H); ^{13}C NMR (50 MHz, DMSO- d_6) δ (ppm): 104.77, 123.81, 124.00, 126.23, 126.71, 127.93, 128.31, 128.55, 130.40, 132.77, 133.50, 141.89, 149.21, 163.07.

4.1.2.15. 5-((1,1'-Biphenyl)-4-yl)-1H-pyrazole-3-carboxylic acid (15). Starting from 0.50 g of 4-((1,1'-biphenyl)-2-yl)-2,4-dioxobutanoic acid, 0.42 g of product was obtained (85% of theoretical yield). White solid, mp = 286–287 °C, dec. (hexane/AcOEt); $\text{C}_{16}\text{H}_{12}\text{N}_2\text{O}_2$, $M_w = 264.28$; ESI-MS: Calculated for $\text{C}_{16}\text{H}_{13}\text{N}_2\text{O}_2$ $[\text{M}+\text{H}]^+$: 265.09715, measured: 265.09653; IR (ν , cm^{-1}): 3220 (N–H), 1657 (C=O), 1451, 1275; ^1H NMR (200 MHz, DMSO- d_6) δ (ppm): 7.28 (s, 1H), 7.36 (t, $J = 7.30$ Hz, 1 H), 7.46 (t, $J = 7.86$ Hz, 2 H), 7.69 (d, 2 H, overlapped with doublet at 7.74), 7.74 (d, $J = 7.86$ Hz, 2 H), 7.95 (d, $J = 7.86$ Hz, 2 H), 13.21 (br); ^{13}C NMR (50 MHz, DMSO- d_6) δ (ppm): 105.66, 126.13, 126.84, 127.38, 127.89, 129.28, 130.40, 139.82, 140.00, 147.66, 162.14.

4.1.2.16. 5-(4-(Pyrrolidin-1-yl)phenyl)-1H-pyrazole-3-carboxylic acid (16). Starting from 0.2 g of 4-(4-(pyrrolidin-1-yl)phenyl)-2,4-dioxobutanoic acid, 0.16 g of product was obtained (81% of theoretical yield). Pale red solid, mp = 276–279 °C, dec. (hexane); $\text{C}_{14}\text{H}_{15}\text{N}_3\text{O}_2$, $M_w = 257.29$; ESI-MS: Calculated for $\text{C}_{14}\text{H}_{16}\text{N}_3\text{O}_2$ $[\text{M}+\text{H}]^+$: 258.12370, measured: 258.12359; IR (ν , cm^{-1}): 3207 (N–H), 2963, 1711 (C=O), 1616, 1515, 1189; ^1H NMR (200 MHz, DMSO- d_6) δ (ppm): 1.94 (br, t, 2 H), 3.24 (br, t, 2 H), 6.54 (d, $J = 8.42$ Hz, 2 H), 6.91 (s, 1 H), 7.60 (d, $J = 8.42$ Hz, 2 H), 8.91 (br); ^{13}C NMR (50 MHz, DMSO- d_6) δ (ppm): 25.17, 47.48, 103.04, 111.91, 118.28, 126.46, 142.10, 147.67, 147.94, 163.24.

4.1.2.17. 5-(4-Fluorophenyl)-1H-pyrazole-3-carboxylic acid (17). Starting from 0.58 g of 4-(4-fluorophenyl)-2,4-dioxobutanoic acid, 0.37 g of product was obtained (65% of theoretical yield). White solid, mp = 227–228 °C (hexane/AcOEt); $\text{C}_{10}\text{H}_7\text{FN}_2\text{O}_2$, $M_w = 206.17$; ESI-MS: Calculated for $\text{C}_{10}\text{H}_8\text{FN}_2\text{O}_2$ $[\text{M}+\text{H}]^+$: 207.05643, measured: 207.05643; IR (ν , cm^{-1}): 3334 (N–H), 3091, 1659 (C=O), 1453, 1240; ^1H NMR (200 MHz, DMSO- d_6) δ (ppm): 7.24 (s, 1 H), 7.30 (t, $^3J_{\text{HH}} = 8.42$ Hz, $^3J_{\text{HF}} = 8.99$ Hz, 2H), 7.92 (dd, $^3J_{\text{HH}} = 8.42$ Hz, $^4J_{\text{HF}} = 5.05$ Hz, 2 H) 11.81–14.42 (s, br); ^{13}C NMR (50 MHz, DMSO- d_6) δ (ppm): 105.57, 115.84, 116.28, 127.56, 127.73, 128.20, 139.38, 147.74, 159.84, 161.92, 164.71.

4.1.2.18. 5-(4-Chlorophenyl)-1H-pyrazole-3-carboxylic acid (18). Starting from 0.27 g of 4-(4-chlorophenyl)-2,4-dioxobutanoic acid, 0.23 g of product was obtained (87% of theoretical yield). White solid, mp = 256–257 °C (hexane/AcOEt); $\text{C}_{10}\text{H}_7\text{ClN}_2\text{O}_2$, $M_w = 222.63$; ESI-MS: Calculated for $\text{C}_{10}\text{H}_8\text{ClN}_2\text{O}_2$ $[\text{M}+\text{H}]^+$: 223.02688, measured: 223.02694; IR (ν , cm^{-1}): 3188 (N–H), 1679 (C=O), 1488, 1271; ^1H NMR (200 MHz, DMSO- d_6) δ (ppm): 8.47 (s, 1 H) 8.71 (d, $J = 8.42$ Hz, 2 H) 9.10 (d, $J = 8.99$ Hz, 2 H); ^{13}C NMR

(50 MHz, DMSO- d_6) δ (ppm): 105.86, 127.29, 129.18, 130.62, 132.88, 161.76, two low-intensity signals from pyrazole C=N and C–NH not observed.

4.1.2.19. 5-(3-Bromophenyl)-1H-pyrazole-3-carboxylic acid (19). Starting from 0.57 g of 4-(3-bromophenyl)-2,4-dioxobutanoic acid, 0.45 g of product was obtained (80% of theoretical yield). White solid, mp = 249–251 °C (hexane/AcOEt); $\text{C}_{10}\text{H}_7\text{BrN}_2\text{O}_2$, $M_w = 267.08$; ESI-MS: Calculated for $\text{C}_{10}\text{H}_8\text{BrN}_2\text{O}_2$ $[\text{M}+\text{H}]^+$: 266.97637, measured: 266.97587; IR (ν , cm^{-1}): 3246 (N–H), 1694 (C=O), 1462, 1304; ^1H NMR (200 MHz, DMSO- d_6) δ (ppm): 7.35 (s, 1 H), 7.42 (t, $J = 7.30$ Hz, 1 H), 7.55 (d, $J = 7.30$ Hz, 1 H), 7.90 (d, $J = 7.86$ Hz, 1 H), 8.09 (s, 1 H), 13.43 (br); ^{13}C NMR (50 MHz, DMSO- d_6) δ (ppm): 106.23, 122.61, 124.58, 125.58, 128.00, 129.20, 131.04, 131.33, 161.70.

4.1.2.20. 5-(4-Hydroxyphenyl)-1H-pyrazole-3-carboxylic acid (20). Starting from 0.46 g of 4-(4-hydroxyphenyl)-2,4-dioxobutanoic acid, 0.39 g of product was obtained (87% of theoretical yield). White solid, mp = 282–283 °C, dec. (hexane/AcOEt); $\text{C}_{10}\text{H}_8\text{N}_2\text{O}_3$, $M_w = 204.18$; ESI-MS: Calculated for $\text{C}_{10}\text{H}_9\text{N}_2\text{O}_3$ $[\text{M}+\text{H}]^+$: 205.06077, measured: 205.05983; IR (ν , cm^{-1}): 3290 (N–H), 1679 (C=O), 1616, 1514, 1265; ^1H NMR (200 MHz, DMSO- d_6) δ (ppm): 6.85 (d, $J = 8.42$ Hz, 2 H), 7.04 (s, 1 H), 7.67 (d, $J = 8.42$ Hz, 2 H), 9.80 (br) 12.90 (br); ^{13}C NMR (50 MHz, DMSO- d_6) δ (ppm): 104.31, 115.95, 122.01, 127.07, 141.07, 147.50, 157.90, 162.63.

4.1.2.21. 5-(2-Methoxyphenyl)-1H-pyrazole-3-carboxylic acid (21). Starting from 0.40 g of 4-(2-methoxyphenyl)-2,4-dioxobutanoic acid, 0.29 g of product was obtained (74% of theoretical yield). White solid, mp = 234–235 °C (hexane/AcOEt); $\text{C}_{11}\text{H}_{10}\text{N}_2\text{O}_3$, $M_w = 218.21$; ESI-MS: Calculated for $\text{C}_{11}\text{H}_{11}\text{N}_2\text{O}_3$ $[\text{M}+\text{H}]^+$: 219.07642, measured: 219.07644; IR (ν , cm^{-1}): 3270, (N–H), 1708 (C=O), 1470, 1179; ^1H NMR (200 MHz, DMSO- d_6) δ (ppm): 3.91 (s, 3 H), 7.05 (t, $J = 7.30$ Hz, 1 H) 7.13 (d, overlapped with singlet at 7.17, 1 H), 7.17 (s, 1 H), 7.37 (t, $J = 8.42$, 1 H), 7.83 (dd, $J_{1,2} = 7.86$ Hz, $J_{1,3} = 1.68$ Hz, 1 H), 13.27 (br). ^{13}C NMR (50 MHz, DMSO- d_6) δ (ppm): 55.76, 108.19, 112.18, 118.79, 120.97, 127.98, 129.91, 141.22, 142.86, 156.19, 162.98.

4.1.2.22. 5-(4-Methoxyphenyl)-1H-pyrazole-3-carboxylic acid (22). Starting from 0.50 g of 4-(4-methoxyphenyl)-2,4-dioxobutanoic acid, 0.45 g of product was obtained (92% of theoretical yield). White solid, mp = 226–228 °C, dec. (hexane/AcOEt); $\text{C}_{11}\text{H}_{10}\text{N}_2\text{O}_3$, $M_w = 218.21$; ESI-MS: Calculated for $\text{C}_{11}\text{H}_{11}\text{N}_2\text{O}_3$ $[\text{M}+\text{H}]^+$: 219.07642, measured: 219.07540; IR (ν , cm^{-1}): 3309, 3249 (N–H), 1679 (C=O), 1456, 1206; ^1H NMR (200 MHz, DMSO- d_6) δ (ppm): 3.77 (s, 3 H) 6.99 (d, $J = 8.99$ Hz, 2 H), 7.09 (s, 1 H), 7.76 (d, $J = 8.42$ Hz, 2 H), 13.21 (br); ^{13}C NMR (50 MHz, DMSO- d_6) δ (ppm): 55.45, 104.75, 114.60, 123.70, 127.00, 140.62, 147.45, 159.57, 162.43.

4.1.2.23. 5-(4-Methoxy-2,5-dimethylphenyl)-1H-pyrazole-3-carboxylic acid (23). Starting from 0.62 g of 4-(4-methoxy-2,5-dimethylphenyl)-2,4-dioxobutanoic acid, 0.54 g of product was obtained (89% of theoretical yield). Pale yellow solid, mp = 232–234 °C, dec. (hexane/AcOEt); $\text{C}_{13}\text{H}_{14}\text{N}_2\text{O}_3$, $M_w = 246.26$; ESI-MS: Calculated for $\text{C}_{13}\text{H}_{15}\text{N}_2\text{O}_3$ $[\text{M}+\text{H}]^+$: 247.10772, measured: 247.10769; IR (ν , cm^{-1}): 3304, 3164 (N–H), 1695 (C=O), 1510, 1430, 1238; ^1H NMR (200 MHz, DMSO- d_6) δ (ppm): 2.14 (s, 3 H), 2.36 (s, 3 H), 3.81 (s, 3 H), 6.81 (s, 1 H), 6.87 (s, 1 H), 7.27 (s, 1 H), 13.08 (br); ^{13}C NMR (50 MHz, DMSO- d_6) δ (ppm): 15.77, 20.96, 55.56, 107.68, 112.89, 122.74, 123.27, 131.17, 134.65, 140.82, 146.27, 157.42, 162.83.

Representative ^1H and ^{13}C NMR spectra are provided in [Supplementary Material, Figures S10–S31](#).

4.1.3. Determination of acidity constant

The acidity constant (pK_{a1}) value of 4-MeO derivative (**22**) was determined using spectrophotometric titration at 25 ± 1 °C. The 50.0 ml of 1×10^{-4} M working solution was prepared in 10 mM phosphate buffer, pH = 1.73, $I = 0.1$ M (NaCl) and titrated with 1 M KOH till pH 6 was reached (total volume change was less than 1% at the end of titration). UV/Vis spectra were recorded in 220–420 nm range against the phosphate buffer as a blank. pK_{a1} Value was calculated according to equation:²⁷

$$A_{\lambda} = \frac{A_{\lambda(A^{-})} - A_{\lambda}}{[H_3O^{+}]} \cdot K_{a1} + A_{\lambda(HA)} \quad (1)$$

where $A_{\lambda(A^{-})}$ is the absorbance of pure deprotonated compound ($-COO^{-}$), $A_{\lambda(HA)}$ is absorbance of molecular form ($-COOH$), and A_{λ} is the absorbance of solutions at different pH values where both forms of compound **22** exist in the solution.

4.2. CA Inhibition

An SX.18MV-R Applied Photophysics stopped-flow instrument was used for assaying the CA-catalyzed CO_2 hydration activity by using the method of Khalifah.²⁸ Inhibitor and enzyme were preincubated for 15 min prior to assay. IC_{50} values were obtained from dose response curves working at seven different concentrations of test compound (from 0.1 nM to 100 μ M), by fitting the curves using PRISM (www.graphpad.com) and non-linear least squares methods. The obtained values represent the mean of at least three different determinations, as described earlier by us.^{29,30} The inhibition constants (K_i) were then derived by using the Cheng–Prusoff equation, as follows: $K_i = IC_{50}/(1 + [S]/K_m)$, where [S] represents the CO_2 concentration at which the measurement was carried out, and K_m the concentration of substrate at which the enzyme activity is at half maximal. All enzymes used were recombinant, produced in *Escherichia coli* as reported earlier.^{31–34} The concentrations of enzymes used in the assay were: hCA I, 12.3 nM; hCA II, 7.7 nM; hCA IX, 9.9 nM and hCA XII, 12.3 nM.

4.3. Molecular modeling

Structures of compounds **1–23**, in its anionic form, were prepared in SMILES notation (simplified molecular-input line-entry system). Both tautomers A and B (Scheme 2) were considered. Conformers of the each compound was generated in OMEGA 2.4.3,³⁵ using MMFF94s force field (build and search) and default settings.³⁶ With the exception of the 4-*n*-Bu derivative (**4**), conformational assemblies per molecule did not exceed 50 conformations. The use MMFF94s force field without Coulomb interaction (NoEstat); and/or decrease of root-mean-square (rms) value of atomic positions between conformers that should be included in conformational assembly, comparing to OMEGA default settings, did not produced more conformers per molecule. Carbonic anhydrases were modeled from the following PDB entries: CA I–1HCB, CAII–3BF4, CAIX–3IAI and CAXII–1JD0. The one subunit (subunit A), of the CAIX and CAXII was used, and water and other small molecules were removed from all structures used for modelling. Protonation states of His residues was adopted from PDB entry 4G0C,³⁷ obtained by neutron diffraction. His64 was treated as a neutral, with protonated delta N. In the input PDB files, protonation states of histidine residues were specified by appropriate residue names, following CHARMM convention (HSD or HSE). Hydrogens of other atoms are ascribed automatically during proteins preparation using CHARMM-GUI.³⁸ Protonation states of ionizable residues other than His was subsequently visually checked and compared with protonation states of 4G0C structure. Each protein was neutralized by addition of counter-ions and embedded in water sphere surrounding protein by 10 Å layer from the edges.

CHARMM36 parameters were ascribed by CHARMM-GUI. Each protein was submitted to three cycles of minimization (minimization–heating–minimization...) during 20 ps each, without any restrains, in NAMD2.9.³⁹ Conjugate gradient minimizer was used. In this way obtained protein structures were used for docking studies and for comparison of active sites. For docking studies Zn-bound water molecule was added. Docking of compounds **1–23** to all four proteins were performed by FRED 3.0.1^{40,41} with docking resolution set to high, without any constraint. The whole protein, considered as the receptor, was prepared in OpenEye ‘MakeReceptor’ graphical user interface. Both His64 ‘in’ and ‘out’ conformation was considered in each protein, in separate docking runs. Ten top-ranked docking solutions were used for analysis. For the comparison of active sites proteins are aligned by their α -traces using DaliLight web interface.^{42,43} GRID²⁶ molecular interaction fields (MIFs) with hydrophobic (DRY), HBD (N1), and HBA (O) probes, were calculated in FLAP2.1.^{44,45} Grid resolution was set to 0.5 Å. MIFs were calculated in the box encompassing following residues (1JD0 residues numbering): Trp5, Thr60, Asn62, His64, Lys67, Asn69, Gln92, His94, His96, His119, Val121, Ala131, Ser132, Thr133, Ala134, Val143, Leu198, Thr199, Thr200, Pro202 and the Zn^{2+} ion, for the each protein and having exactly the same size. Box used for the GRID calculation, along with the important residues labeled, on the example of hCA XII, is depicted in Supplementary Material, Figure S9. The same box and the field of DRY probe on isocontour level of -0.7 kcal/mol is enclosed as a PyMol state file (Supplementary Material, file 2). The 3D-dependent whole molecular properties (Surface area, Polar surface area, Apolar surface area, Volume and VirtualLog P^{46}) of compounds **1–23** in its anionic forms were calculated in VegaZZ 3.0.5⁴⁷ from structures optimized by semiempirical molecular-orbital PM6 method,⁴⁸ as applied in MOPAC2012.⁴⁹ For the calculation of 3D-dependent molecular properties, probe with radius of 0 Å was used. VegaZZ were also used for handling of protein structures and for set-up and analysis of MD calculations. MD and docking calculations were performed on Linux-based multi-node clusters equipped with the Intel Xeon E5345, or X5560 processors.⁵⁰ Figures from FLAP or FRED outputs were prepared in PyMol 1.7.0⁵¹ or VIDA 4.2.1. 2D depictions provided in Supplementary Material were made by OpenEye OEDepictTK.

Acknowledgements

Ministry of Education, Science, and Technological Development of Serbia (Grant No. 172035) and EU FP7 grants (Metoxia and Dynano projects for CTS) supported this work. Authors gratefully acknowledge OpenEye Scientific Software, Santa Fe, NM, for the free, academic, licensing of software tools. Authors gratefully acknowledge computational time provided on HPCG and PARADOX-III high-performance computing facilities. HPCG cluster is located at the Institute of Information and Communication Technologies of the Bulgarian Academy of Science (IICT-BAS). PARADOX-III is located at the Scientific Computing Laboratory, Institute of Physics, Belgrade, and supported by national and EU grants.

Supplementary data

Supplementary data associated with this article can be found, in the online version, at <http://dx.doi.org/10.1016/j.bmc.2015.05.052>.

References

- van Herk, T.; Brussee, J.; van den Nieuwendijk, A. M. C. H.; van der Klein, P. A. M.; Ijzerman, A. P.; Stannek, C.; Burmeister, A.; Lorenzen, A. J. *Med. Chem.* **2003**, *46*, 3945.

2. Frank, A. O.; Feldkamp, M. D.; Kennedy, J. P.; Waterson, A. G.; Pelz, N. F.; Patrone, J. D.; Vangamudi, B.; Camper, D. V.; Rossanese, O. W.; Chazin, W. J.; Fesik, S. W. *J. Med. Chem.* **2013**, *56*, 9242.
3. Liu, G.; Xin, Z.; Pei, Z.; Hajduk, P. J.; Abad-Zapatero, C.; Hutchins, C. W.; Zhao, H.; Lubben, T. H.; Ballaron, S. J.; Haasch, D. L.; Kaszubska, W.; Rondinone, C. M.; Trevillyan, J. M.; Jirousek, M. R. *J. Med. Chem.* **2003**, *46*, 4232.
4. *PubChem bio-assays*: AID 1012 (uHTS identification of TNAP inhibitors in the absence of phosphate acceptor performed in luminescent assay, Burnham Center for Chemical Genomics) and AID 1056 (SAR analysis of an In Vitro TNAP Dose Response Luminescent Assay, Burnham Center for Chemical Genomics).
5. Sechi, M.; Innocenti, A.; Pala, N.; Rogolino, D.; Carcelli, M.; Scozzafava, A.; Supuran, C. T. *Bioorg. Med. Chem. Lett.* **2012**, *22*, 5801.
6. Maresca, A.; Temperini, C.; Vu, H.; Pham, N. B.; Poulsen, S.-A.; Scozzafava, A.; Quinn, R. J.; Supuran, C. T. *J. Am. Chem. Soc.* **2009**, *131*, 3057.
7. Maresca, A.; Temperini, C.; Pochet, L.; Masereel, B.; Scozzafava, A.; Supuran, C. T. *J. Med. Chem.* **2010**, *53*, 335.
8. Maresca, A.; Supuran, C. T. *Bioorg. Med. Chem. Lett.* **2010**, *20*, 4511.
9. Maresca, A.; Scozzafava, A.; Supuran, C. T. *Bioorg. Med. Chem. Lett.* **2010**, *20*, 7255.
10. D'Ambrosio, K.; Carradori, S.; Monti, S. M.; Buonanno, M.; Secci, D.; Vullo, D.; Supuran, C. T.; De Simone, G. *Chem. Commun.* **2015**, 302.
11. Davis, R. A.; Hofmann, A.; Osman, A.; Hall, R. A.; Mühlischlegel, F. A.; Vullo, D.; Innocenti, A.; Supuran, C. T.; Poulsen, S.-A. *J. Med. Chem.* **2011**, *54*, 1682.
12. von Gnielinski, N.; Nienaber, L.; Mason, L.; Ellis, S.; Triccas, J. A.; Davis, R. A.; Hofmann, A. *MedChemComm* **2014**, *5*, 1563.
13. Martin, D. P.; Cohen, S. M. *Chem. Comm.* **2012**, 5259.
14. Innocenti, A.; Vullo, D.; Scozzafava, A.; Casey, J. R.; Supuran, C. T. *Bioorg. Med. Chem. Lett.* **2005**, *15*, 573.
15. Boztaş, M.; Çetinkaya, Y.; Topal, M.; Gülçin, İ.; Menzek, A.; Şahin, E.; Tanç, M.; Supuran, C. T. *J. Med. Chem.* **2015**, *58*, 640.
16. Sof'ina, O. A.; Igidov, N. M.; Koz'minykh, E. N.; Trapeznikova, N. N.; Kasatkina, Yu. S.; Koz'minykh, V. O. *Russ. J. Org. Chem.* **2001**, *37*, 1017.
17. Zhang, X.-Y.; Liu, W.; Tang, W.; Lai, Y.-B. *Acta Crystallogr. E* **2007**, *E63*, o3764.
18. ADMET Predictor, Version 7.1; Simulations Plus, 2014, <http://www.simulations-plus.com>.
19. Alterio, V.; Di Fiore, A.; D'Ambrosio, K.; Supuran, C. T.; De Simone, G. *Chem. Rev.* **2012**, *112*, 4421.
20. Kumar, V.; Kannan, K. K. *J. Mol. Biol.* **1994**, *241*, 226.
21. Güzel, Ö.; Temperini, C.; Innocenti, A.; Scozzafava, A.; Salman, A.; Supuran, C. T. *Bioorg. Med. Chem. Lett.* **2008**, *18*, 152.
22. Alterio, V.; Hilvo, M.; Di Fiore, A.; Supuran, C. T.; Pan, P.; Parkkila, S.; Scaloni, A.; Pastorek, J.; Pastorekova, S.; Pedone, C.; Scozzafava, A.; Monti, S. M.; De Simone, G. *Proc. Natl. Acad. Sci. U.S.A.* **2009**, *106*, 16233.
23. Whittington, D. A.; Waheed, A.; Ulmasov, B.; Shah, G. N.; Grubb, J. H.; Sly, W. S.; Christianson, D. W. *Proc. Natl. Acad. Sci. U.S.A.* **2001**, *98*, 9545.
24. Supuran, C. T. *Nat. Rev. Drug Disc.* **2008**, *7*, 168.
25. Güzel-Akdemir, Ö.; Akdemir, A.; Isik, S.; Vullo, D.; Supuran, C. T. *Bioorg. Med. Chem.* **2013**, *21*, 1386.
26. Goodford, P. J. *J. Med. Chem.* **1985**, *28*, 849. <http://www.moldiscovery.com/software/grid/>.
27. Albert, A.; Serjeant, E. P. *The Determination of Ionization Constants*, 2nd ed.; Chapman and Hall: London, 1971; p 44.
28. Khalifah, R. J. *J. Biol. Chem.* **1971**, *246*, 2561.
29. Maresca, A.; Vullo, D.; Scozzafava, A.; Manole, G.; Supuran, C. T. *J. Enzyme Inhibit. Med. Chem.* **2013**, *28*, 392.
30. Maresca, A.; Scozzafava, A.; Vullo, D.; Supuran, C. T. *J. Enzyme Inhibit. Med. Chem.* **2013**, *28*, 384.
31. Scozzafava, A.; Menabuoni, L.; Mincione, F.; Mincione, G.; Supuran, C. T. *Bioorg. Med. Chem. Lett.* **2001**, *11*, 575.
32. Vomasta, D.; Innocenti, A.; König, B.; Supuran, C. T. *Bioorg. Med. Chem. Lett.* **2009**, *19*, 1283.
33. Supuran, C. T.; Maresca, A.; Gregáň, F.; Remko, M. *J. Enzyme Inhibit. Med. Chem.* **2013**, *28*, 289.
34. Allouche, F.; Chabchoub, F.; Carta, F.; Supuran, C. T. *J. Enzyme Inhibit. Med. Chem.* **2013**, *28*, 343.
35. Hawkins, P. C. D.; Skillman, A. G.; Warren, G. L.; Ellingson, B. A.; Stahl, M. T. *J. Chem. Inf. Model.* **2010**, *50*, 572. <http://www.eyesopen.com/omega>.
36. Halgren, T. A. *J. Comput. Chem.* **1999**, *20*, 720.
37. Fisher, S. Z.; Aggarwal, M.; Kovalevsky, A. Y.; Silverman, D. N.; McKenna, R. J. *Am. Chem. Soc.* **2012**, *134*, 14726.
38. Jo, S.; Kim, T.; Iyer, V. G.; Im, W. *J. Comput. Chem.* **1859**, *2008*, 29.
39. Phillips, J. C.; Braun, R.; Wang, W.; Gumbart, J.; Tajkhorshid, E.; Villa, E.; Chipot, C.; Skeel, R. D.; Kalé, L.; Schulten, K. S. *J. Comput. Chem.* **2005**, *26*, 1781. <http://www.ks.uiuc.edu/Research/namd/>.
40. McGann, M. R.; Almond, H. R.; Nicholls, A.; Grant, J. A.; Brown, F. K. *Biopolymers* **2003**, *68*, 76.
41. McGann, M. *J. Chem. Inf. Model.* **2011**, *51*, 578. <http://www.eyesopen.com/oedocking>.
42. Goujon, M.; McWilliam, H.; Li, W.; Valentin, F.; Squizzato, S.; Paern, J.; Lopez, R. *Nucleic Acids Res.* **2010**, *38*, W695.
43. Holm, L.; Park, J. *Bioinformatics* **2000**, *16*, 566.
44. Baroni, M.; Cruciani, G.; Sciabola, S.; Perruccio, F.; Mason, J. S. *J. Chem. Inf. Model.* **2007**, *47*, 279. <http://www.moldiscovery.com/software/flap/>.
45. Cross, S.; Baroni, M.; Goracci, L.; Cruciani, G. *J. Chem. Inf. Model.* **2012**, *52*, 2587.
46. Gaillard, P.; Carrupt, P. A.; Testa, B.; Boudon, A. *J. Comput. Aided Mol. Des.* **1994**, *8*, 83.
47. Pedretti, A.; Villa, L.; Vistoli, G. *J. Comput. Aided Mol. Des.* **2004**, *18*, 167. <http://ddl.unimi.it>.
48. Stewart, J. J. P. *J. Mol. Model.* **2007**, *13*, 1173.
49. Stewart, J. J. P. *J. Comput. Aided Mol. Des.* **1990**, *4*, 1. MOPAC2012, Stewart Computational Chemistry, Colorado Springs, CO, USA. <http://OpenMOPAC.net>.
50. Atanassov, E.; Gurov, T.; Karaivanova, A. *Autom. Inf.* **2011**, *2*, 7.
51. The PyMol Molecular Graphics System, Version 1.7.1.3, Schrodinger LLC.